Hydrology and Earth System Sciences, 3(4), *463–476* (1999) © EGS

Hydrology & Earth System Sciences

Implementing surface parameter aggregation rules in the CCM3 global climate model: regional responses at the land surface

M.A. Arain[1], E.J. Burke, Z.-L. Yang and W.J. Shuttleworth

Department of Hydrology and Water Resources, The University of Arizona, Tucson AZ 85721 USA
email for corresponding author: shuttle@hwr.arizona.edu
[1] Now at Department of Soil Sciences, University of British Columbia, Vancouver, V6T 1Z4, Canada

Abstract

The land-surface parameters required as input to a GCM grid box (typically a few degrees) are often set to be those of the dominant vegetation type within the grid box. This paper discusses the use and effect of aggregation rules for specifying effective values of these land cover parameters by taking into account the relative proportion of each land-cover type within each individual grid box. Global land-cover classification data at 1 km resolution were used to define Biosphere Atmosphere Transfer Scheme (BATS) specific aggregate (using aggregation rules) land-cover parameters. Comparison of the values of the aggregate parameters and those defined using the single dominant vegetation type (default parameters) shows significant differences in some regions, particularly in the semi-desert and in forested regions, e.g. the Sahara Desert and the tropical forest of South America. These two different sets of parameters were used as input data for two 10-year simulations of the NCAR CCM3 model coupled to the BATS land-surface scheme. Statistical analyses comparing the results of the two model runs showed that the resulting effects on the land-surface diagnostics are significant only in specific regions. For example, the sensible heat flux in the Sahara Desert calculated for the aggregate parameter run increased due to the marked increase in the minimum stomatal resistance and the decrease in fractional vegetation cover in the aggregate parameters over the default parameters. The modelled global precipitation and surface air temperature fields were compared to observations: there is a general improvement in the performance of the aggregate parameter run over the default parameter run in areas where the differences between the aggregate and default parameter run are significant. However, most of the difference between the modelled and observed fields is attributable to other model deficiencies. It can be concluded that the use of aggregation rules to derive land-surface parameters results in significant changes in modelled climate and in some improvements in the land-surface diagnostics in selected regions. There is also some evidence that there is a response in the global circulation pattern, which is a focus of further work.

Introduction

Surface-cover parameters are known to play an important role in Soil-Vegetation-Atmosphere Transfer Schemes (SVATS), particularly in the movement of energy and water (Dickinson and Henderson-Sellers, 1988; Rowntree, 1991; Garratt, 1993). SVATS are used to parameterise the lower boundary conditions of atmospheric General Circulation Models (GCMs), which can be used for both numerical weather prediction and climate simulation. Hence, an accurate representation of the lower boundary condition, i.e. the land-surface cover, is an essential component of any GCM. However, at the grid scale of a GCM (typically between $1° \times 1°$ and $3° \times 3°$), the land-surface cover can be strongly heterogeneous. This issue is neglected in most GCM studies with just the dominant surface cover for each grid taken to provide a representative parameterisation. This paper examines the impact on the land-surface diagnostics of using aggregated surface cover parameters, more representative of a natural, heterogeneous cover, within a GCM grid cell.

Significant progress has been made recently in the definition of heterogeneous vegetation cover within atmospheric model grid cells at both local and regional scales (Mason, 1988; Koster and Suarez, 1992; Wood and Mason, 1991; Blyth *et al.*, 1993; Lynn *et al.*, 1995; Raupach and Finnigan, 1995, 1997; Arain *et al.*, 1996, 1997; and Shuttleworth *et al.*, 1997). Methods of aggregating the vegetation parameters, which are used to define the grid-average energy and water fluxes, are generally

divided into two categories. The first is the so called tiled or mosaic approach which couples patches of each vegetation present within a grid cell with the overlying atmosphere at each time step and then averages the energy and water fluxes over the entire grid (Koster and Suarez, 1992; Raupach and Finnigan, 1995). The second approach uses simple, hypothetical aggregation rules to derive grid-average surface-cover parameters based on the fractional cover area of all the component vegetation cover types present in a grid cell (Shuttleworth, 1991). The aggregation rules are such that the surface energy fluxes are similar to those found using an explicit representation of the individual patches of vegetation. The advantage of the 'aggregation rule approach' is that this method is computationally efficient: aggregate parameters are calculated prior to the model runs from high-resolution land-cover classes.

Arain *et al.* (1996, 1997) applied simple aggregation rules at both the FIFE site in Kansas and an ABRACOS site in Brazil. They coupled an advanced land-surface parameterisation, the Biosphere-Atmosphere-Transfer Scheme (*BATS*; Dickinson *et al.*, 1993) with a two-dimensional Atmospheric Boundary Layer Model (Mason and Sykes, 1980) and used the resulting model to test hypothetical aggregation schemes using meteorological and soil-moisture observations. The same simple aggregate rules were used to derive aggregate values of vegetation parameters across the United States using remotely sensed land-cover classes at 1 km resolution. These aggregate parameters were then tested with a standalone version of *BATS* and two years of International Satellite Land Surface Climatology Project (ISLSCP) 'Initiative-One' forcing data (Arain *et al.*, 1997). Results of all of these studies showed that, in most cases, a weighted-linear averaging rule is effective. However, if the fluxes are not proportional to the parameters (e.g. in the case of aerodynamic roughness length), alternative averaging procedures are required.

Theoretical work by McNaughton (1994), Raupach (1995), and Raupach and Finnigan (1995, 1997) demonstrated that the well-accepted equations which describe surface-atmosphere exchanges at smaller homogeneous plot scales e.g. the Penman-Monteith equation (Monteith, 1965) can also be used to describe the area-average behaviour of heterogeneous cover at larger scales. However, these equations require information on surface and aerodynamic resistance (and hence the meteorological variables) at each time step and therefore cannot be applied to models that operate in a free-running predictive mode. Shuttleworth *et al.* (1997) and Shuttleworth (1999) combined the above-mentioned theoretical aggregation approach with empirical aggregation rules to provide a new aggregation scheme that is computationally efficient and based on theory. This theory-based aggregation approach is adopted here to derive aggregate values of two of the more important vegetation parameters, i.e. aerodynamic roughness length (z_0) and minimum stomatal resistance ($r_{s,\min}$).

In this paper, the aggregation approach of Shuttleworth *et al.* (1997) and Arain *et al.* (1996, 1997) is adopted. The aggregation approach was evaluated using version 3 of the National Center for Atmospheric Research's (NCAR's) Community Climate Model (*CCM3*) coupled with *BATS* and a 1 km resolution global land-cover classification from the Earth Resources Observing System Data Center Distributed Active Archive (EDC-DAAC). Here, the focus is on the response of the land-surface diagnostics over the regions that are strongly influenced by the changes in vegetation parameter values derived using the aggregation rules.

New Aggregation Approach

The Penman-Monteith equation (Monteith, 1965) is currently used in most weather and climate prediction models to describe evaporation. It is a resistance-based model which assumes that water vapour first diffuses out of the leaves against the stomatal resistance and then onward into the overlying atmosphere against the aerodynamic resistance (Shuttleworth, 1993). This equation allows the calculation of evaporation using meteorological variables and the stomatal and aerodynamic resistance of the surface vegetation cover. McNaughton (1994), Raupach (1995), and Raupach and Finnigan (1995, 1997) used the Penman-Monteith equation to represent surface energy partitioning at both the patch and grid scale. They related the aerodynamic resistance and the surface resistance at the grid scale to those at the patch scale using two assumptions. Their first assumption is that the area-average scalar fluxes are conserved. Secondly, they assumed that the 'model' used to describe area-average land-surface/atmosphere exchanges at the grid-scale must have the same form as the 'model' used to describe the exchanges at the patch scale (McNaughton, 1994). These two assumptions provide an elegant and accurate theoretical link between the resistances at different scales. However, they require knowledge of the patch-specific atmospheric variables and of the soil moisture. Therefore, this linking mechanism cannot be used in free-standing, predictive climate models (Shuttleworth *et al.*, 1997). Shuttleworth *et al.* (1997) combined these theoretical linking procedures with the empirical aggregation approach taken by Mason (1988), Shuttleworth (1991), Blyth *et al.* (1993), Noilhan and Lacarrére (1995) and Arain *et al.* (1996, 1997) to define aggregation equations for the two key land-surface cover parameters not well represented by the empirical approach, i.e. z_0 and $r_{s,\min}$. This aggregation approach—'the theory-based approach'—is discussed in detail by Shuttleworth *et al.* (1997) and, for completeness, summarised below.

The theory-based aggregation rules require information about the natural land-surface cover types present within

a model grid cell at the patch scale (e.g. from remotely sensed surface-cover classes at 1 km resolution). The theory-based approach for roughness length (z_0) gives:

$$\ln^{-2}\left(\frac{(z_b - d)}{z_0}\right) = \sum_i w_i \ln^{-2}\left(\frac{(z_b - d_i)}{z_{0i}}\right) \quad (1)$$

where z_b is the 'blending height' (previously defined by Wierenga (1986), Mason (1988), and Arain *et al.* (1996)); i is the patch number within the grid cell; w_i is the fractional area of patch i in the grid cell; z_0 is the zero plane displacement; and d is the displacement height given by Arain *et al.* (1997):

$$d = \sum_i w_i d_i \quad (2)$$

The theory-based approach for the minimum stomatal resistance ($r_{s,\min}$) gives:

$$r_{s,\min} = l_{grid} \frac{\sum_i \left[\frac{w_i \rho_i}{(\Delta + 1) + \rho_i}\right]}{\sum_i \left[\frac{w_i / r_{a,i}}{(\Delta + 1) + \rho_i}\right]} \quad (3)$$

where ($\Delta = [(\lambda / c_p) dq_{sat}/dT]$ is the dimensionless slope of the saturation specific humidity (q_{sat}) as a function of air temperature (T); λ is the latent heat of vaporisation of water; and c_p is specific heat of air. The leaf area index of the grid (l_{grid}) is given by the area-weighted average of the individual leaf area indices (L_i) (Arain *et al.*, 1996):

$$l_{grid} = \sum_i w_i L_i \quad (4)$$

and ρ_i is given by:

$$\rho_i = \frac{k^2 U_b r_{s,\min,i}}{L_i \ln^2\left(\frac{(z_b - d_i)}{z_{0,i}}\right)} \quad (5)$$

where k is the von Karman constant, and U_b is the grid average wind speed estimated at the 'blending height' (z_b). The aerodynamic resistance of patch i($r_{a,i}$) is given by:

$$r_{a,i} = \frac{\ln^2\left(\frac{(z_b - d_i)}{z_{0,i}}\right)}{k^2 U_b} \quad (6)$$

The calculation of grid average values of $r_{s,\min}$ requires the grid-average values of leaf area index (Eqn. 4). In *BATS*, the leaf area, L_i, of each cover class is a function of maximum and minimum values of leaf area index, $L_{i,\max}$ and $L_{i,\min}$ respectively and of the deep ground temperature (T_g in K). This allows for seasonal changes in L_i. Therefore, in *BATS*, the following equation is used to calculate L_i:

$$L_i = L_{i,\max} + [L_{i,\min} - L_{i,\max}](1 - S') \quad (7)$$

where

$$S' = S(T_g) \quad S(T) > 0$$
$$S' = 0 \quad S(T_g) \le 0 \quad (8a)$$

and

$$S(T_g) = 1 - 0.0016 T_{g,\max}^2 \quad (8b)$$

with $T_{g,\max} = (298 - T_g)$ or zero, whichever is greater.

Matrials and Methods

BIOSPHERE-ATMOSPHERE TRANSFER SCHEME (*BATS*)

BATS is a comprehensive SVAT scheme designed for use in the NCAR CCMs (Dickinson *et al.*, 1993). It is based on our current understanding of biological processes at the patch scale. *BATS* consists of separate model components that describe radiative and hydrological interactions. The soil is divided into three layers for water balance calculations, and the model recognises the separate contributions of soil and vegetation to surface fluxes. The model describes two transfer phases in the movement of water and heat flux from the canopy to the atmosphere. Firstly, it represents the exchange with the air within the canopy and, secondly, the exchange between the canopy air and the overlying atmosphere. The processes considered within the canopy are sensible and latent heat exchange with the atmosphere, absorption of solar radiation, and the influence of the presence of canopy surface moisture, which may be present as a result of dew or rainfall. Over dry areas of the canopy, stomatal resistance controls the escape of water to the adjacent external air from within the leaf by assuming that the air inside the leaf is saturated. Stomatal resistance increases as soil moisture decreases.

BATS calculates latent and sensible heat fluxes using the classical equations where the sensible heat flux is proportional to the temperature gradient between the surface and the air and where the latent heat flux is proportional to the humidity gradient. Ground heat flux is calculated as a residual from the surface energy balance, and soil temperature is calculated using the force-restore method (Dickinson, 1988). All surface fluxes are proportional to the drag coefficient, which is a function of the height of the lowest atmospheric model level.

BATS has 18 land surface-cover types which are based on data sets of Olson *et al.* (1983), Matthews (1983), and Wilson and Henderson-Sellers (1985). Each surface-cover type has 15 associated parameters that describe the physical, morphological and physiological properties of the land cover. There are 12 soil types, ranging from very coarse sand (= 1) to very fine clay (= 12), and eight soil colours ranging from light (= 1) to dark (= 8).

COMMUNITY CLIMATE MODEL VERSION 3 (*CCM3*)

This study uses version 3 of the Climate Community Model (*CCM3*) developed by the NCAR Climate and Global Dynamic (CGD) Division. *CCM3* is a comprehensive state-of-the-art GCM designed to allow understanding and analysis of the global climate system. It has 18 vertical levels which extend up to the 2.90 mbar level and a horizontal grid of approximately 3° × 3°. Kiehl *et al.* (1996) described the physical parameterisation and numerical algorithms used in the model, and Acker *et al.* (1996) presented details of the code, data structure and model use.

Many aspects of *CCM3* are similar to version 2 (*CCM2*, Hack *et al.*, 1993). However, in addition to enhanced computational efficiency, *CCM3* contains improved model physics and improved dynamical formulations, particularly for the atmospheric boundary layer and hydrological processes. *CCM3* offers an optional slab, mixed-layer/sea ice formulation that makes it suitable for most global change studies. Optional message-passing configuration allows the model to run in parallel mode in distributed-memory environments. In this study, the version of *CCM3* that is linked to *BATS* (Dickinson *et al.*, 1993) was adopted because *BATS* has been used extensively in past aggregation studies at various field sites (Arain *et al.*, 1996, 1997; White *et al.*, 1997).

At each time step, the atmospheric model provides *BATS* with incident solar radiation, incident long-wave radiation, convective and large-scale precipitation plus the near surface wind speed, air temperature, specific humidity and pressure (calculated at the lowest atmospheric model level). *BATS* returns surface albedo, upward long-wave radiation, sensible heat, latent heat, water vapour flux and the surface stresses to the atmospheric model. Simulations using *CCM3-BATS* provide an excellent opportunity to test the performance of the new theory-based aggregation rules at 3° × 3° resolution.

CALCULATION OF GLOBAL AGGREGATE PARAMETERS

The global land-surface cover classification data used to define the aggregate parameters for input into *CCM3-BATS* were obtained from the EDC-DAAC (EDC-DAAC). These data were generated jointly by the U.S. Geological Survey, the University of Nebraska-Lincoln and the European Commission's DG Joint Research Centre. They used Advanced Very High Resolution Radiometer (AVHRR) data spanning April 1992 through March 1993 to generate surface-cover classification data at 1 km resolution on a continent-by-continent basis. Monthly AVHRR Normalised Difference Vegetation Index (*NDVI*) maximum value composites for April 1992 through March 1993 were used to define seasonal greenness classes. The translation of the seasonal greenness classes to land cover classification requires additional data including digital elevation, ecoregions data and a collection of other land-cover/vegetation reference data (Loveland *et al.*, 1991, 1997). Classification data for six different land-classifying systems were derived and made available, including the system used within *BATS*.

The fractional area of each *BATS* surface-cover type within each *CCM3* grid box (3° × 3° resolution) was calculated using the 1 km EDC-DAAC data set (*BATS* category). Each *BATS* surface-cover type was assigned its 15 associated parameters (Dickinson *et al.*, 1993). Aggregate values of 13 of the 15 *BATS* vegetation parameters (except $r_{s,\min}$ and z_0) were calculated for each *CCM3* grid box using a linear averaging rule based on the fractional area of each cover type within a model grid as in Eqn. 2 (Shuttleworth, 1991; Arain *et al.*, 1996;1997; Shuttleworth *et al.*, 1997).

The aggregate values of the aerodynamic roughness length (z_0) and the minimum stomatal resistance ($r_{s,\min}$) were calculated using the new theory-based aggregation rules given in Eqns. 1 and 3, respectively. Calculation of aggregate values of z_0, and $r_{s,\min}$ requires a knowledge of the wind speed, air temperature and pressure at the blending height (for the calculation of Δ in Eqn. 3) and the deep soil temperature. The monthly average values of the blending height and of the other meteorological data required were calculated for each *CCM3* model grid from a 'default' 11-year *CCM3-BATS* simulation. This default *CCM3-BATS* simulation uses the dominant land cover in each *CCM3* grid box to define the 15 *BATS* associated parameters. The lowest modelled level, typically around 60 m (± 5 m) above the land surface, was taken to represent the blending height. Aggregate values of z_0 and $r_{s,\min}$ were then calculated for each month using the monthly mean meteorological data; this was to capture the seasonal behaviour of these two parameters. Finally, time-averaged aggregate values of z_0 and $r_{s,\min}$ were calculated for each model grid cell.

CCM3-BATS MODEL RUNS

The effects of using aggregate land-surface parameters on the modelled climate were studied by comparing results from two multi-year *CCM3-BATS* simulations. The first default parameter run used a single-cover type (for the dominant land cover within each CCM3 grid cell) to define the 15 *BATS* parameters. This default model was run for an 11-year simulation. The second aggregate parameter run was initiated at the end of year 1 of the default parameter run and then run for 10 more years. This procedure was designed to minimise the effects of initialisation on the modelled climate. The simulated climate for the final 10 years of these two runs was then compared.

Comparison of Aggregate and Dominant Cover Parameters

A comparison of the global aggregate land-cover parameters (calculated using the methodology described above, with the global default land-cover parameters (calculated using a single cover type—the dominant land cover for each *CCM3* grid box) reflects the much greater spatial variation in the aggregate parameters relative to the default parameters. For example, in the boreal forests of North America, the dominant cover type is needleleaf tree. However, the high-resolution land-cover data show that there are areas of shorter vegetation interspersed within the forest; these influence the effective grid-average parameters to an extent which depends on the proportion present within each grid cell. A similar situation occurs in the Amazon where the dominant type is broadleaf tree.

Figure 1 shows the differences between the aggregate and default land-cover parameters for six representative surface-cover parameters: minimum stomatal resistance ($r_{s,\min}$); minimum leaf area index ($LAI_{\min}$); albedo (α); fractional vegetation cover (σ_f); aerodynamic roughness length (z_0); and zero plane displacement height (d). These differences are illustrated in terms of the percentage difference between the aggregate and default parameters relative to the mean of the aggregate and default parameters. The percentage differences are greater than 10% for well over half of the land area and are commonly of the order of 20–60%, although in selected regions the percentage difference is as great as 100% or more, e.g. $LAI_{\min}$ in the Sahara Desert. In general, the most notable differences occur in the semi-desert and forested regions, where there are patches of vegetation included within the aggregate representation that have characteristics which contrast strongly with those of the dominant vegetation type. There are also particularly noticeable changes in coastal regions—this is because of the inclusion of areas of water in the calculation of the effective grid parameters.

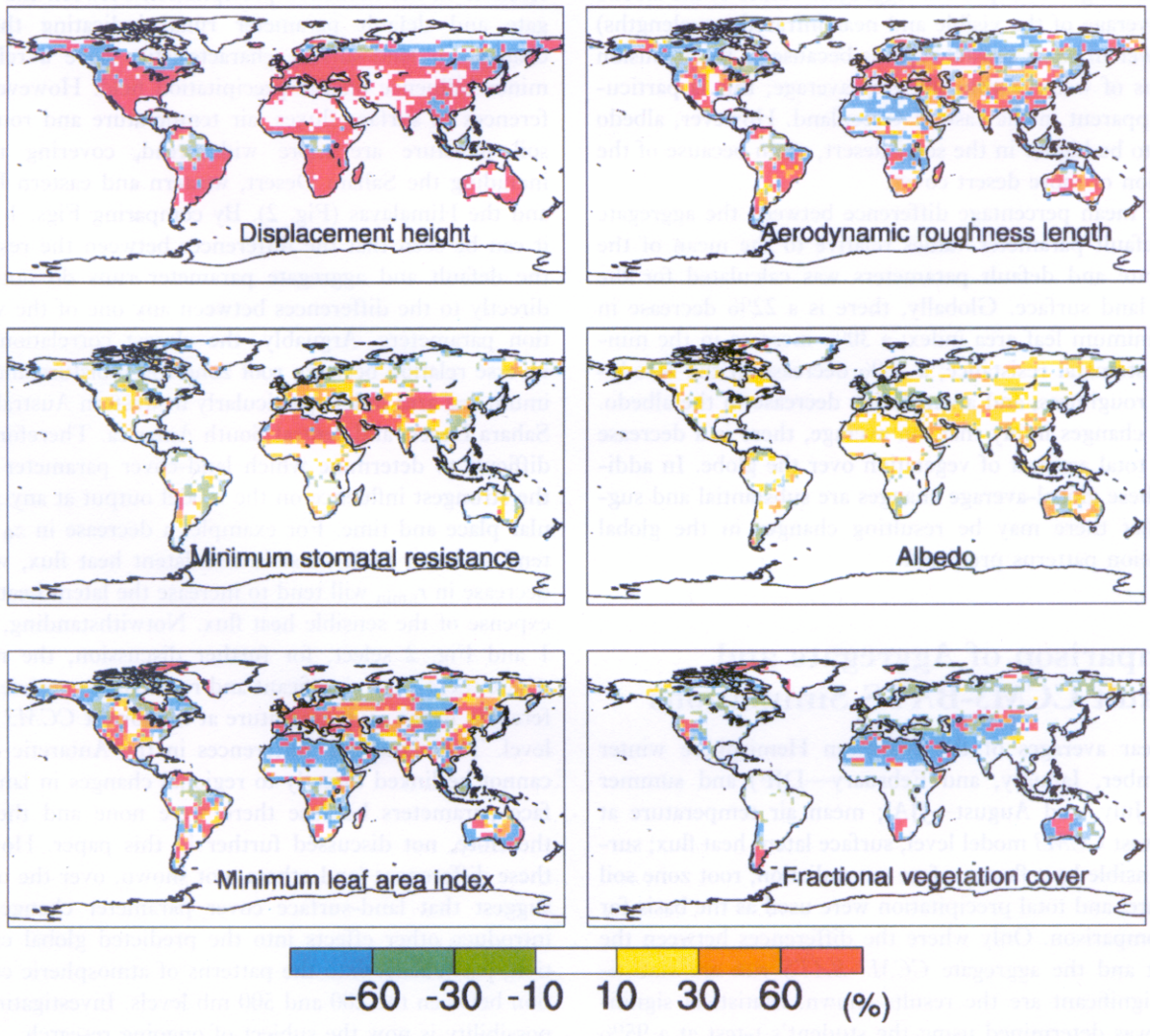

Fig. 1. *Difference between BATS-relevant aggregate vegetation parameters derived from the USGS/EDC data and the single dominant vegetation cover values assigned in CCM3 grid cells (3° × 3°) expressed as a percentage of the mean of the aggregate and default.*

Patches of shorter vegetation within the tropical forests of South America and Africa and the boreal forests of North America lower the aggregate values of both the zero plane displacement (d) and the aerodynamic roughness length (z_0) by between 20–80%. Similarly, there is a decrease in fractional vegetation cover (σ_f) and minimum leaf area index ($LAI_{\min}$) over these forested regions. In many other vegetated regions, the aggregate values of d and z_0 increase by 40–200% because of the inclusion of patches of taller vegetation. The aggregate values of σ_f and $LAI_{\min}$ also increase by a similar amount. In the semi-desert regions, for example in North Africa, aggregate values of σ_f and $LAI_{\min}$ generally decrease because of the inclusion of more desert cover. However, in a few particular desert grid boxes, more vegetation in the aggregate cover compared to the default cover results in an increase of σ_f and $LAI_{\min}$. On the average, areas with higher aggregate values of σ_f and $LAI_{\min}$ tend to have lower aggregate values of minimum stomatal resistance ($r_{s,\min}$) and vice-versa, as might be expected. Aggregate values of the albedo (α – average of the visible and near infrared wavelengths) are lower in some coastal regions because of the inclusion of areas of water within the grid average; this is particularly apparent in the case of Greenland. However, albedo tends to be higher in the semi-desert, again because of the inclusion of more desert cover.

The mean percentage difference between the aggregate and default parameter values relative to the mean of the aggregate and default parameters was calculated for the entire land surface. Globally, there is a 22% decrease in the minimum leaf area index; a 30% increase in the minimum stomatal resistance; a 36% decrease in the aerodynamic roughness; and a small, 5% decrease in the albedo. These changes imply that, on average, there is a decrease in the total amount of vegetation over the globe. In addition, these global-average changes are substantial and suggest that there may be resulting changes in the global circulation patterns predicted.

Comparison of Aggregate and Default CCM3-BATS Simulations

Ten-year averages of the Northern Hemisphere winter (December, January, and February—DJF) and summer (June, July, and August—JJA); mean air temperature at the lowest *CCM3* model level; surface latent heat flux; surface sensible heat flux; surface net radiation; root zone soil moisture; and total precipitation were used as the basis for this comparison. Only where the differences between the default and the aggregate *CCM3-BATS* run are statistically significant are the results shown. Statistical significance was determined using the student's t-test at a 95% confidence level (Chervin and Schneider, 1976). At each grid point the significance of the difference between the means of the aggregate and default model run was assessed based on the standard deviation of the 10 yearly samples within each 10 year run. Figure 2 shows the differences between the aggregate and default parameter runs for JJA. The oceans were masked in addition to the regions where the two model runs were not significantly different. Results from DJF (not shown) show similar patterns; however, the areas where the differences are statistically significant are smaller and the differences are themselves less. The reduction in land area over which changes were significant in DJF as compared to JJA reflects the greater land mass in the Northern Hemisphere over which the conditions are more extreme during JJA.

The first thing to note from Fig. 2 is that the default and aggregate parameter runs are not significantly different over the entire land surface, only in certain regions of the globe. This is despite the fact that there is a large change in the global averages of the aggregate parameters when compared to the default parameters. There are only a few very scattered regions where there are significant differences in the modelled precipitation between the aggregate and default parameter runs, indicating that the changes in land-surface characteristics have a relatively minor influence on the precipitation field. However, differences in surface fluxes, air temperature and root zone soil moisture are more widespread, covering regions including the Sahara Desert, western and eastern Europe and the Himalayas (Fig. 2). By comparing Figs. 1 and 2, it can be seen that the differences between the results of the default and aggregate parameter runs do not relate directly to the differences between any one of the vegetation parameters. Arguably, the closest correlation is an inverse relation between root zone soil moisture and minimum leaf area index, particularly in western Australia, the Sahara Desert and central South America. Therefore, it is difficult to determine which land-cover parameter exerts the strongest influence on the model output at any particular place and time. For example, a decrease in z_0 might tend to lower both sensible and latent heat flux, while a decrease in $r_{s,\min}$ will tend to increase the latent heat at the expense of the sensible heat flux. Notwithstanding, Table 1 and Fig. 2 select, for further discussion, the regions where there were significant and reasonably consistent differences in the air temperature at the lowest *CCM3* model level. The significant differences in the Antarctic clearly cannot be linked directly to regional changes in land-surface parameters because there were none and they are, therefore, not discussed further in this paper. However, these differences (and others, not shown, over the oceans) suggest that land-surface cover parameter changes may introduce other effects into the predicted global circulation, particularly into the patterns of atmospheric circulation between the 200 and 500 mb levels. Investigating this possibility is now the subject of ongoing research.

Tables 2 and 3 respectively show the differences between the 10-year mean values for the aggregate and default parameter runs for the Northern Hemisphere sum-

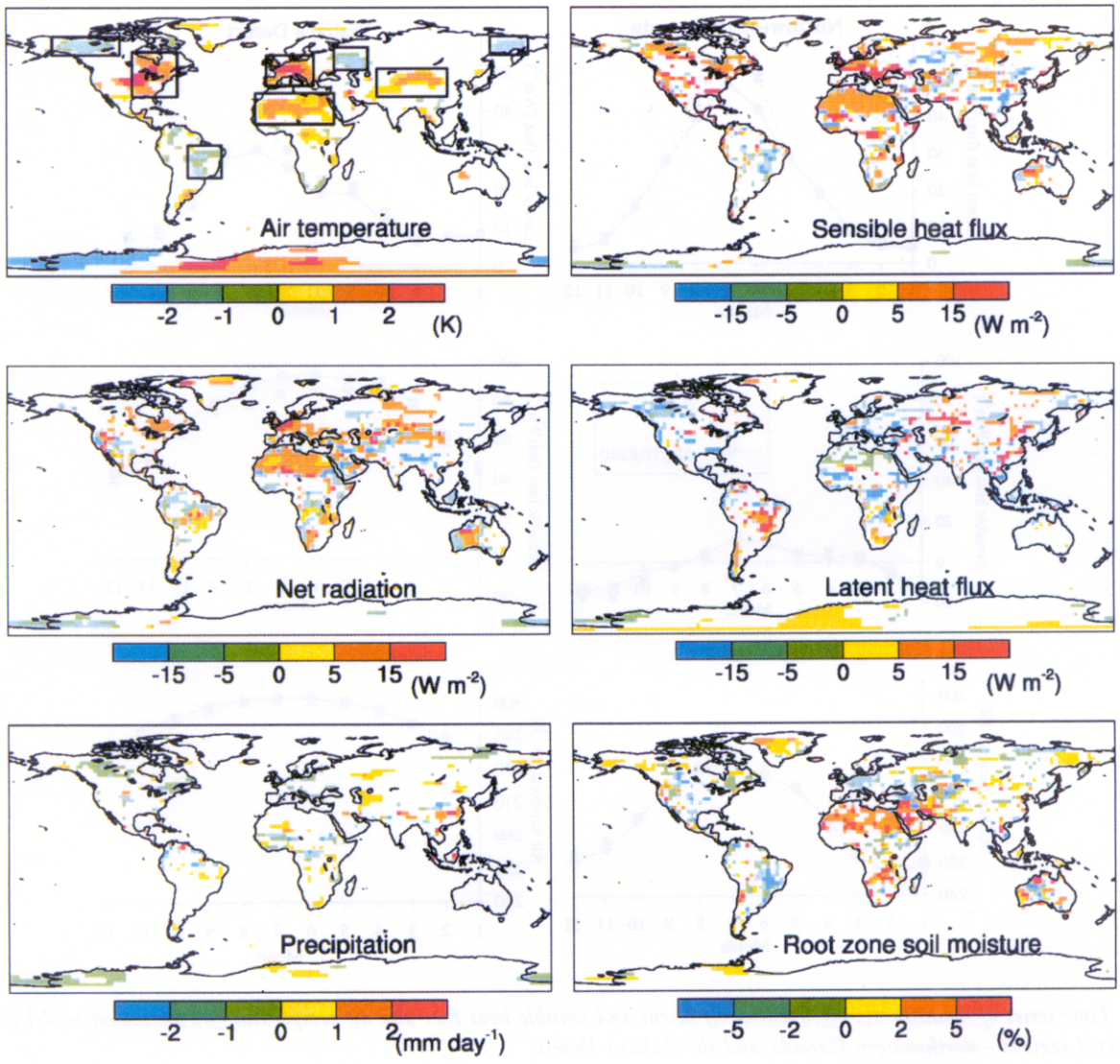

Fig. 2. *Difference between the aggregate and default of the land-surface diagnostics for the Northern Hemisphere summer (June-July-August (JJA)). Only the regions where the differences are significant (at the 95% level) are shown. Regions selected for further analysis are highlighted in the air temperature figure.*

Table 1. Locations of the regions where the air temperature at the lowest *CCM3* model level is significantly different between default and aggregate parameter runs. These are the regions selected for further analysis.

Region	North (°N)	South (°N)	East (°E)	West (°E)
Northwestern Canada	80	55	–110	–155
Great Lakes Region	60	25	–65	–100
Central South America	–2	–28	–40	–65
Western Europe	60	35	27	–10
Sahara Desert	30	12	37	–12
Eastern Europe	62	47.5	62	32
Himalayas	48	30	115	58
Eastern Russia	70	66	165	140

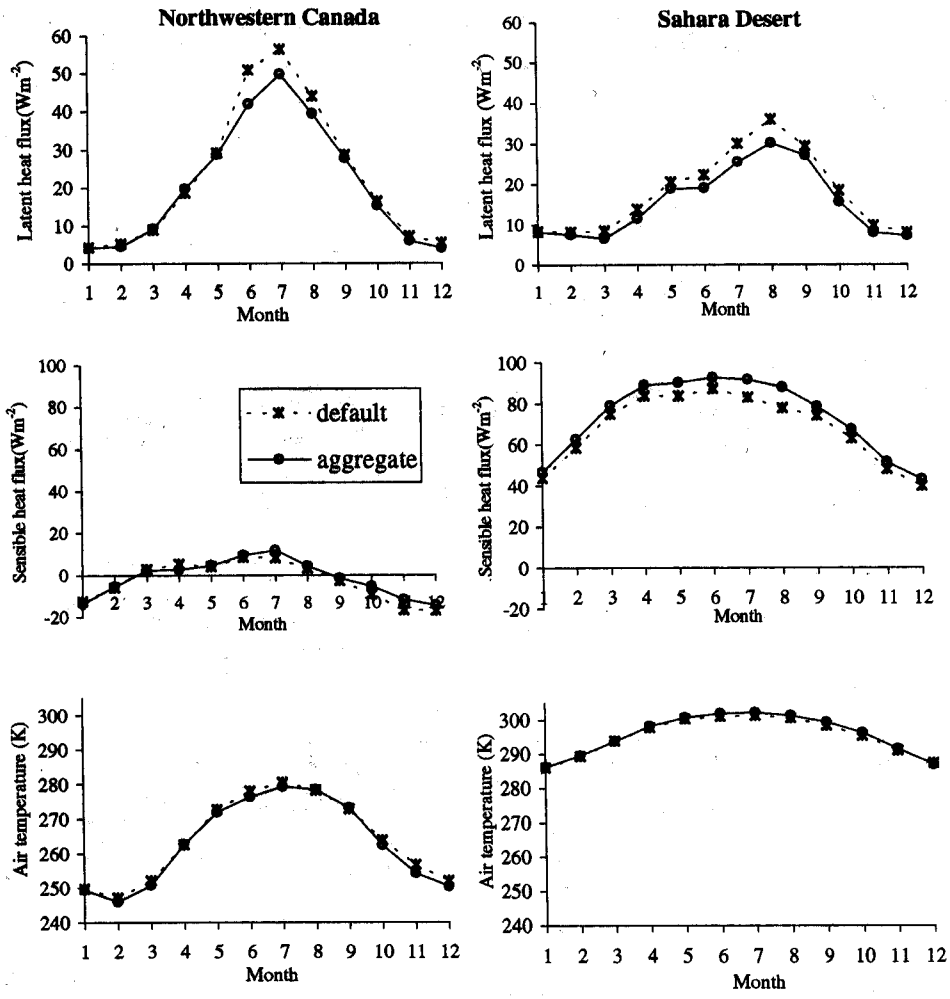

Fig. 3. *Time series of monthly averaged values of latent and sensible heat flux and air temperature at the lowest model level for two selected regions—northwestern Canada and the Sahara Desert.*

Table 2. Difference between the land-surface diagnostics for the 10-year averages of aggregate and default parameter runs for Northern Hemisphere summer (JJA) for the regions selected in Table 1.

Region (JJA)	Air temperature at 1st model level (K)	Sensible heat flux (W m^{-2})	Latent heat flux (W m^{-2})	Net radiation (W m^{-2})	Root zone soil moisture (%)
Northwestern Canada	–0.83	1.98	–6.67	–2.15	0.8
Great Lakes Region	1.48	8.34	–4.02	4.13	–0.6
Central South America	–0.49	–4.57	5.06	0.63	–1.7
Western Europe	1.09	9.32	–6.74	6.48	–0.6
Sahara Desert	0.84	8.11	–4.60	3.68	2.3
Eastern Europe	–0.72	–3.60	–0.99	–3.64	0.1
Himalayas	0.64	1.69	–0.38	1.19	0.1
Eastern Russia	–1.33	1.47	–3.16	–2.94	1.4

Table 3. Difference between the land surface diagnostics for the 10-year averages of aggregate and default parameter runs for Northern Hemisphere winter (DJF) for the regions selected in Table 1.

Region (DJF)	Air temperature at 1st model level (K)	Sensible heat flux (W m^{-2})	Latent heat flux (W m^{-2})	Net radiation (W m^{-2})	Root zone soil moisture (%)
Northwestern Canada	–1.10	0.73	–0.72	0.04	0.6
Great Lakes Region	1.53	–0.39	–0.15	–0.94	0.0
Central South America	–0.07	–2.41	2.83	0.26	–0.6
Western Europe	0.15	–0.69	2.10	–0.01	–0.4
Sahara Desert	0.05	3.55	–0.50	2.89	2.1
Eastern Europe	–3.70	–0.56	0.45	0.49	0.1
Himalayas	–0.20	–1.39	–0.08	–1.42	0.3
Eastern Russia	–1.33	0.82	–0.23	0.42	1.6

mer (JJA) and winter (DJF) for the regions defined in Table 1 and shown in Fig. 2. Table 4 shows the percentage difference between selected aggregate and default parameters relative to the mean of the aggregate and default parameters for the same regions. Precipitation is neglected in this discussion because Fig. 2 shows that the only continuous region of significant difference is in northwestern Canada. In the Sahara Desert, the Great Lakes region, western Europe and the Himalayas, there is an increase in air temperature and sensible heat flux, net radiation, and corresponding decrease in latent heat flux. This is consistent with the decrease in the amount of vegetation present as indicated by the decrease in *LAI* and σ_f and increase in $r_{s,\min}$ (Table 4). The significant increase in root zone soil moisture in the Sahara Desert is also consistent with less vegetation. There are minimal changes in root zone soil moisture in the other three regions. In central South America, an increase in latent heat flux and a decrease in air temperature and sensible heat flux and root zone soil moisture but only a minimal change in net radiation is consistent with the increase in vegetation indicated by a slight increase in *LAI* and a slight decrease in $r_{s,\min}$. The changes discussed above can be associated directly with the change in canopy cover. However, in eastern Europe, northwestern Canada and eastern Russia, parameter changes exert opposing influences on land-surface diagnostics. It is possible, for instance, that in eastern Europe, the decrease in z_0 lowers both the latent and sensible heat flux and dominates the slight increase in $r_{s,\min}$.

Figure 3 provides further insight. It shows the time series of 10-year monthly averaged values of sensible and latent heat flux and air temperature at the first *CCM3* model level for two regions, namely the Sahara Desert and northwestern Canada. In the Sahara Desert, the sensible heat flux given with default parameters is smaller than that given with aggregate parameters for the entire year, results for air temperature are similar. In northwestern Canada, the default air temperature is greater than the aggregate air temperature for the entire year, as also is the latent heat flux. However, the default sensible heat flux is greater than the aggregate sensible heat flux in the spring, while for the rest of the year the converse is true. Similar results are seen in the case of eastern Russia. Perhaps current unexplained changes in global circulation patterns are confusing the influence of regional surface controls in this case. Future research will investigate this and related issues.

Table 4. Percentage difference between aggregate and default surface-cover parameters divided by the mean of the aggregate and default surface-cover parameters for the regions selected in Table 1.

Region	$LAI_{\min}$ (%)	$LAI_{\max}$ (%)	f_c (%)	$r_{s,\min}$ (%)	d (%)	z_0 (%)	albedo (%)
northwestern Canada	–45.6	–10.0	–8.5	–4.3	–115.9	–50.0	0.0
Great Lakes Region	–29.3	–10.4	–10.8	–7.2	–37.4	–20.7	6.1
Central South America	1.5	18.3	–1.2	–8.7	–7.0	2.9	0.0
western Europe	17.8	–12.7	–19.8	1.6	200.0	34.1	–6.1
Sahara Desert	–110.3	–111.1	–50.0	68.7	200.0	–40.0	11.8
eastern Europe	8.3	4.5	–1.2	0.8	153.1	–5.1	0.0
Himalayas	–13.9	1.1	–40.0	93.3	–120.0	0.0	8.7
eastern Russia	22.7	–8.6	–10.4	16.8	–117.4	–113.6	6.1

Comparison of CCM3-BATS Simulations with Observations

It is interesting to investigate whether the significant regional changes in the surface diagnostics described above result in an improvement in the *CCM3-BATS* model simulations when compared with observations. The modelled results were compared with observations of both precipitation and air temperature at reference height from Legates and Willmott (1990a, b). [Note: Bonan (1998) compared *CCM3* (including the standard land-surface scheme) with these same observations. The results obtained from the default *CCM3-BATS* model run were comparable to those obtained by Bonan (1998). There are some regions where the results from the two models compare well with observations and some regions where they compare less favourably.]

Figure 4 shows the relative improvement (or not) of the modelled climate given by the *CCM3-BATS* model run using aggregate cover parameters over default cover parameters when compared to observations. The value shown is the modulus of the difference between the aggregate

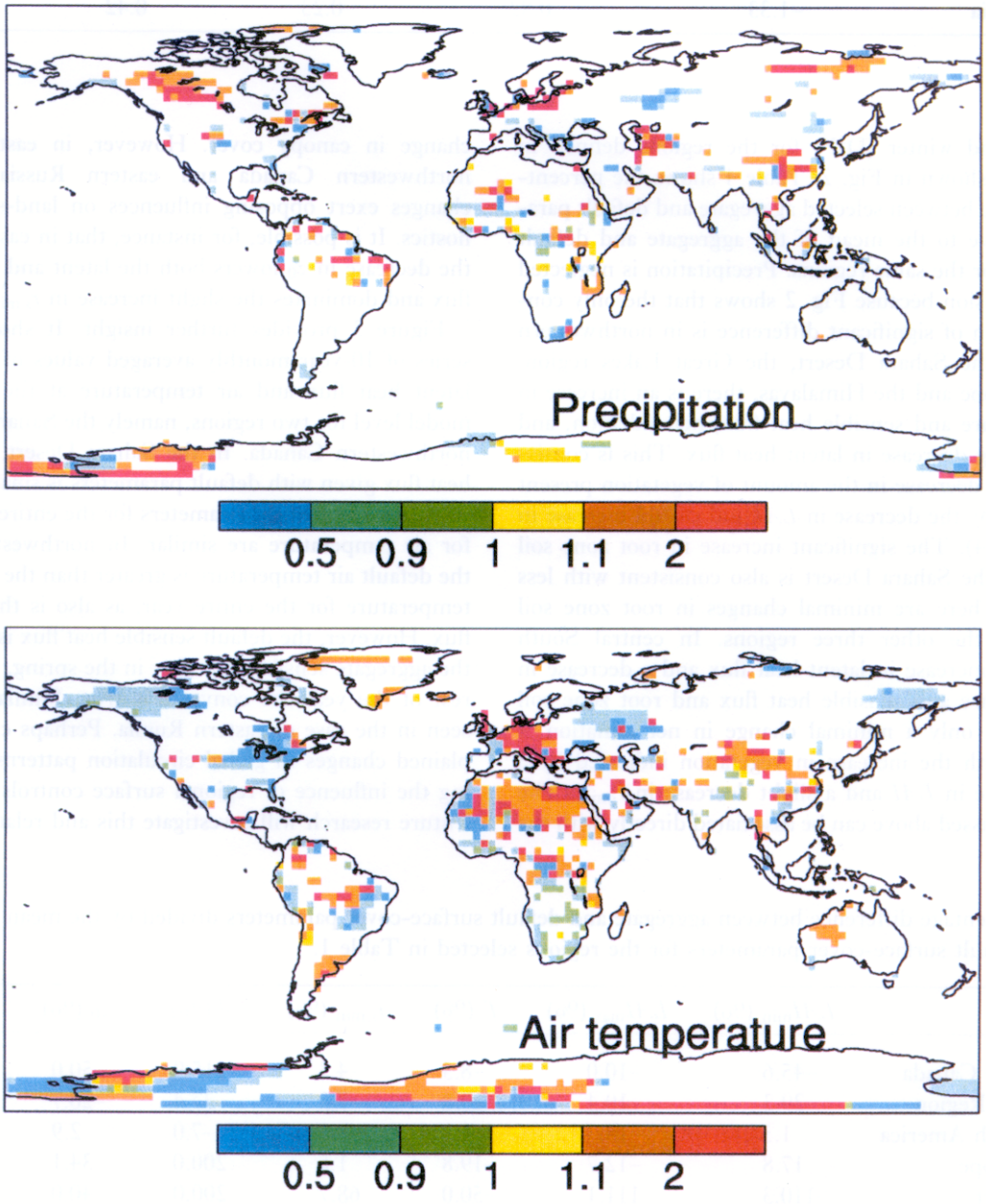

Fig. 4. *Relative improvement of the aggregate model over the default model compared to observations. Only the regions where the differences are significant (at the 95% level) are shown.*

cover parameter run and observations divided by the difference between the default cover parameter run and observations. A value greater than 1 shows improvement. Again, only regions over the land surface where the changes in the precipitation and reference height air temperature were statistically significant are shown for JJA. There is a general tendency for the aggregate parameter run to compare more favourably with observations than the default parameter run. However, this is not true in every region where the difference is significant. The two main regions where there is improvement in modelled precipitation are northwestern Canada and western Europe. However, as mentioned earlier, the modelled change in precipitation tends to be discontinuous. There are improvements in the modelled reference temperature in western Europe, the Sahara and Himalayas, but the modelled reference height air temperature is degraded in northwestern Canada, and eastern Russia. The latter two regions are locations where the change in sensible heat flux indicates that there should have been an increase in the reference level air temperature, and such an increase in air temperature would have resulted in an improved model performance when compared to observations. Again, perhaps changes in the global circulation pattern currently unexplained are confusing the issue in these regions.

Figure 5 shows a time series of the mean monthly reference height air temperature for the eight regions selected

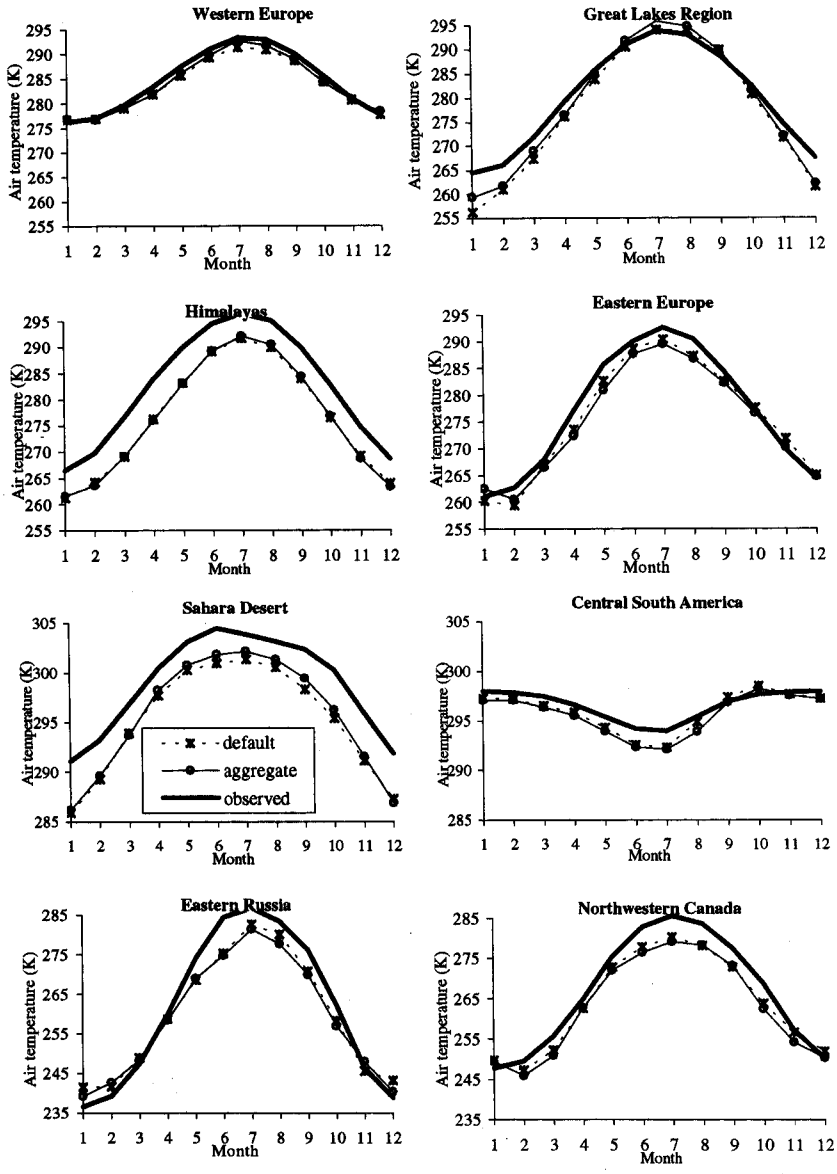

Fig. 5. *Time series of reference height air temperature comparing monthly averaged values of observations with the default and aggregate model runs for selected regions where the differences between the aggregate and default model runs are significant.*

in Table 1. The 10-year mean monthly values for both the default and aggregate parameter runs and the observations are illustrated. The introduction of the aggregate parameters results in a change in the surface diagnostics that is generally very small compared to the difference between the *CCM3-BATS* model and observations. Consequently, the difference between the modelled values and observations is due mainly to model deficiencies other than the specification of land-surface cover parameters. In the locations shown in Fig. 5, there is either a more-or-less favourable comparison with observations, depending on the nature of the difference between modelled values and observations. In some regions such as the Great Lakes, for example, the model results already compare favourably to observations, and the improvement (or otherwise) when aggregate parameters are used depends on the time of year.

Figure 6 shows the time series of monthly mean precipitation for northwestern Canada, western Europe and the Himalayas. Again, the improvement (or otherwise) in the modelled precipitation is small when compared to the differences between the model runs and observations. However, in this case, the model indicates a change in the sign of the difference between aggregate and default parameter runs depending on the time of the year. For example, in northwestern Canada, in the winter with default cover parameters, precipitation is less than with aggregate cover parameters and closer to the observations, whereas in the summer, with default cover parameters, precipitation is greater than with aggregate cover parameters and the aggregate cover parameters give better performance.

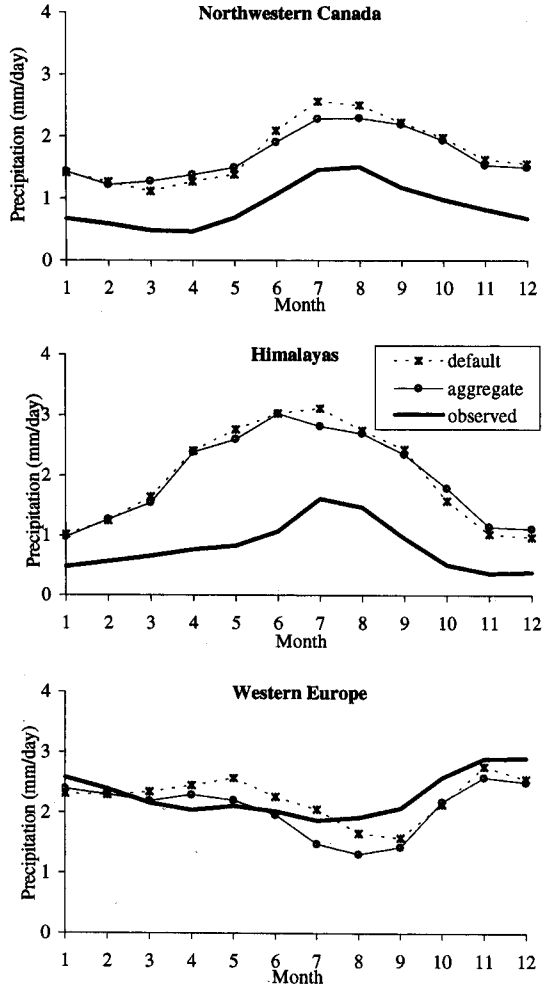

Fig. 6. *Time series of precipitation comparing monthly averaged values of observations with the default and aggregate model runs for selected regions where the differences between the aggregate and default model runs are significant.*

Discussion and Conclusions

In recent years, significant theoretical progress has been made in applying plot scale understanding of surface-atmosphere exchanges to describe the behaviour of heterogeneous surface covers at the much larger grid scale used in climate models. The theory linking these two scales is elegant and exact, but it cannot be applied to climate models that are run in free-standing, predictive mode because it requires knowledge of weather variables at scales less than those used in the climate models. Shuttleworth *et al.* (1997) derived simplified theory-based aggregation rules that calculate area-average parameters at the grid scale used in global climate models. In this study, aggregate land-surface parameters were calculated from these theory-based aggregation rules and remotely sensed land-cover data and used within *CCM3-BATS* to investigate the regional response on the land-surface exchanges and near-surface climate.

Aggregate values of *BATS* vegetation parameters were calculated for a 3° × 3° *CCM3* grid using the aggregation rules with the 1 km EDC-DAAC data set and monthly average values of the required weather variables. The values of the resulting aggregate parameters were then compared with the values for the single most common vegetation cover commonly used within the *CCM3-BATS* grid. There were significant changes in the land-cover parameters both globally (where there was a change on the order of 30% in some key parameters) and regionally. This paper has focused on the regional responses to these modified parameters.

Ten-year simulations using *CCM3-BATS* were carried out with both the dominant cover parameters and the aggregate cover parameters. Significant differences in the modelled land-surface diagnostics between model runs with the default and aggregate cover parameters in certain regions are, in general, not as noticeable or as widespread as might be expected from the very significant differences in the land-surface cover parameters. In the regions where the differences are significant, the difference between the aggregate and default land-surface parameters appears to have a direct influence on the regional differences in, for example, the partitioning of surface energy. In the Sahara

Desert, there is an increase in air temperature and sensible heat flux and a corresponding decrease in latent heat flux consistent with the decrease in leaf area index and fractional vegetation cover in the aggregate compared to the default cover parameters. The opposite effect is true in central South America. However, because of the compounding effect of changing all of the land-surface parameters, in some regions it is difficult to determine which parameter change has the strongest influence on the regional climate. Future research plans include *CCM3-BATS* runs in which surface-cover parameters will be altered independently.

Comparison of the model results with observations showed some statistically significant improvement in the modelled climate with aggregate parameters in some regions. However, there is, in general, little difference between the aggregate parameter and default parameter model runs relative to the substantial difference between both model runs and observations. Presumably this implies that, with *CCM3*, the difference between the modelled and observed surface fields is attributable mainly to model deficiencies other than its specification of land cover.

Finally, there is some evidence of significant differences between the aggregate and default parameter runs in the Antarctic, particularly in the air temperature of the first model level. These differences clearly cannot be attributed to changes in the land-surface parameters because there were none. This leads to the suspicion that changing from default to aggregate parameters may result in changes in the global atmospheric circulation. This exciting possibility is the subject of ongoing research.

Acknowledgements

Primary funding for the research described in this paper was provided under NASA grant number NAG5-3854. Additional support for M. A. Arain came from a NASA Earth System Science Fellowship, grant numbers NGT-30303 and NGT5-30083. Z.-L. Yang was supported by NASA grant number NAG5-3854 and NASA EOS Interdisciplinary Scientific Research Program (U.P.N. 428-81-22 and U.P.N. 429-81-22). The authors acknowledge the EROS Data Center Distributed Active Archive Center (EDC DAAC) and National Center for Atmospheric Research (NCAR) for providing the land-surface cover data set and Community Climate Model version 3, respectively. Appreciation is expressed to Robert E. Dickinson for providing *BATS* and to Soroosh Sorooshian for use of his computational resources. The editorial services provided by Corrie Thies are greatly valued.

References

Acker, T.L., Buja, L.E., Rosinski, J.M. and Truesdale, J.E., 1996. Users' Guide to NCAR *CCM3*, *Tech. Note NCAR/TN-421+IA*, 210pp., National Center for Atmospheric Research, Boulder, CO.

Arain, M.A., Michaud, J.D., Dolman, A.J. and Shuttleworth, W.J., 1996. Testing of vegetation aggregation rules applicable to the Biosphere-Atmosphere Transfer Scheme and the *FIFE* site. *J. Hydrol.*, **177**, 1–22.

Arain, M.A., Shuttleworth, W.J., Yang, Z.-L., Michaud, J.D. and Dolman, A.J., 1997. Mapping surface cover parameters using aggregation rules and remotely sensed cover classes, *Quart. J. Roy. Meteorol. Soc.*, **123**, 2235–2348.

Blyth, E.M., Dolman, A.J. and Wood, N., 1993. Effective resistance to sensible and latent heat flux in heterogeneous terrain, *Quart. J. Roy. Meteorol. Soc.*, **19**, 423–442.

Bonan, G.B., 1998. The land surface climatology of the NCAR land surface model coupled to the NCAR Community Climate Model, *J. Climate*, **11**, 1307–1326.

Chervin, R.M. and Schneider, S.H., 1976. Determining statistical significance of climate experiments with general circulation models, *J. Atmos. Sci.*, **33**, 405–412.

Dickinson, R.E., Henderson-Sellers, A. and Kennedy, P. J., 1993. Biosphere-Atmosphere Transfer Scheme (*BATS*) version 1e for NCAR Community Climate Model, *Tech. Note NCAR/TN-387+STR*, 72pp., National Center for Atmospheric Research, Boulder, CO.

Dickinson, R.E. and Henderson-Sellers, A., 1998. Modelling tropical deforestation: a study of GCM land-surface parameterisations, *Quart. J. Roy. Meteorol. Soc.*, **114**, 439–462.

Dickinson, R.E., 1988. The force-restore model for surface temperature and its generalisations, *J. Climate*, **1**, 1086–1097.

EDC DAAC, Earth resources observing system Data Center Distributed Active Archive Center, *http://edcwww.cr.usgs.gov/landdaac/glcc/glcc.html.*

Garratt, J. R., 1993. Sensitivity of climate simulations to land-surface and atmospheric boundary-layer treatments—a review, *J. Climate*, **6**, 419–449.

Hack, J.J., Boville, B.A., Briegleb, B.P., Kiehl, J.T., Rasch P.J. and Williamson, D.L., 1993. Description of the NCAR Community Climate Model (CCM2), *Tech. Note NCAR/TN-382+STR*, 108pp., National Center for Atmospheric Research, Boulder, CO.

Kiehl, J.T., Hach, J.J., Bonan, G.B., Boville, B.A., Briegleb, B.P., Williamson, D.L. and Rasch, P.J., 1996. Description of the NCAR Community Climate Model (*CCM3*), *Tech. Note NCAR/TN-420+STR*, 152pp., National Center for Atmospheric Research, Boulder, Colorado.

Koster, R.D. and Suarez, M.J., 1992. A comparative analysis of two land surface heterogeneity representations, *J. Climate*, **5**, 1379–1390.

Legates, D.R. and Willmott, C.J., 1990a. Mean seasonal and spatial variability in gage-corrected, global precipitation, *Int. J. Climatol.*, **10**, 111–127.

Legates, D.R. and Willmott, C.J., 1990b. Mean seasonal and spatial variability in global surface air temperature, *Theor. Appl. Climatol.*, **41**, 11–12.

Loveland, T.R., Ohlen, D.O., Brown, J.F., Reed, B.C., Zhu, Z., Merchant, J.W. and Yang, L., 1997. Western hemisphere land cover: progress towards a global land cover characteristics database, in *Proceedings Pecora 13—Human Interventions with the Environment: Prospective from Space.*

Loveland, T.R., Merchant, J.W., Ohlen, D.O. and Brown, J.F., 1991. Development of a land cover characteristics database for the conterminous United States, *Photogram. Eng. Remote Sens.*, **57** 1453–1463.

Lynn, B.H., Rind, D. and Avissar, R., 1995. The impact of mesoscale circulations generated by subgrid-scale landscape

heterogeneities in general circulation models, *J. Climate*, **8**, 191–205.

Mason, P.J. and Sykes, R.I., 1980. A two-dimensional numerical study of horizontal roll vortices in the neutral atmospheric boundary layer. *Quart. J. Roy. Meteorol. Soc.*, **106**, 351–366.

Mason, P.J., 1988. The formation of areally-averaged roughness lengths. *Quart. J. Roy. Meteorol. Soc.*, **114** 399–420.

Matthews, E., 1983. Global vegetation and land use: new high-resolution data bases for climate studies, *J. Climate Appl. Meteor.*, **22**, 474–487.

McNaughton, K.G., 1994. Effective stomatal and boundary layer resistance of heterogeneous surface. *Plant Cell Environ.*, **17**, 1061–1068.

Monteith, J.L., 1965. Evaporation and the environment, *Symp. Soc. Expl. Biol.*, **19**, 205–234.

Noilhan, J. and Lacarrére, P., 1995. GCM gridscale evaporation from mesoscale modeling, *J. Climate* **8**, 206–233.

Olson, J.S., Watts, J.A. and Allison, L.J., 1983. Carbon in live vegetation of major world ecosystems, *DOE/NBB-0037: No. TR004*, 152pp., U. S. Department of Energy, Washington, DC.

Raupach, M.R. and Finnigan, J.J., 1995. Scale issues in boundary-layer meteorology: surface energy balance in heterogeneous terrain, *Hydrol. Process.*, **9**, 589–612.

Raupach, M.R. and Finnigan, J.J., 1997. The influence of topography on meteorological variables and surface-atmosphere interactions, *J. Hydrol.*, **190**, 182–213.

Raupach, M.R., 1995. Vegetation-atmosphere interaction and surface conductance at leaf, canopy and regional scales, *Agric. For. Meteorol.*, **73**, 151–179.

Rowntree, P.R., 1991. Atmospheric parameterization schemes for evaporation over land: basic concepts and climate modeling aspects, in *Land Surface Evaporation, Measurement and Parameterization*, Edited by T. J. Schmugge and J.-C. Andre, pp. 5–29, Springer-Verlag, New York, USA.

Shuttleworth, W.J., Yang, Z.-L. and Arain, M.A., 1997. Aggregation rules for surface parameters in global models, *Hydrol. Earth System Sci.*, **1**, 217–226.

Shuttleworth, W.J., 1999. Combining remotely sensed data using aggregation algorithms, *Hydrol. Earth System Sci.*, **2**, 149–158.

Shuttleworth, W.J., 1993. Evaporation, in *Handbook of Hydrology*, Edited by D. Maidment, pp. 4.1–4.5, McGraw-Hill, Inc.

Shuttleworth, W.J., 1991. The modellion concept, *Rev. Geophys.*, **29**, 585–606.

White, C.B., Houser, P.R., Arain, M.A., Yang, Z.-L., Syed, K. and Shuttleworth, W.J., 1997. The aggregate description of semi-arid vegetation with precipitation-generated soil moisture heterogeneity, *Hydrol. Earth System Sci.*, **1**, 205–212.

Wieringa, J., 1986. Roughness dependent geographical interpolation of surface wind speed averages, *Quart. J. Roy. Meteorol. Soc.*, **112**, 867–889.

Wilson, M.F. and Henderson-Sellers, A., 1985. A global archive of land cover and soil data for use in general circulation models, *J. Climatol.*, **5**, 119–143.

Wood, N. and Mason, P.J., 1991. The influence of static stability on the effective roughness lengths for momentum and temperature, *Quart. J. Roy. Meteorol. Soc.*, **117**, 1025–1056.